Optical Materials 178 (2026) 118241

Contents lists available at ScienceDirect

Optical Materials

journal homepage: www.elsevier.com/locate/optmat

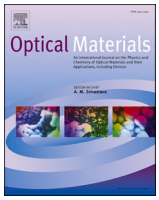

Research Article

# Controlling light polarization using acrylate-based liquid crystal elastomers

Karine Margaryan [a], Gevorg Gevorgyan [a,*], Mariam Hakobyan [a], Tigran Galstian [b], Stuart Berrow [c], Helen Gleeson [c], Rafik Hakobyan [a]

[a] Institute of Physics, Yerevan State University, Yerevan, 0025, Armenia
[b] Laval University, 2375 rue de la Terrasse, Quebec, G1V 0A6, Canada
[c] School of Physics and Astronomy, University of Leeds, Leeds, LS2 9JT, UK

ARTICLE INFO

*Keywords:*
Liquid crystal elastomers
Optical anisotropy
Optical retardation
Waveplates

ABSTRACT

Liquid crystal elastomers (LCEs) are inexpensive, ultrathin, lightweight, soft-elastic, and field-programmable materials enabling the efficient manipulation of light's polarization. In this work, we present procedures for fabricating low-cost, thin-film dielectric quarter-wave and half-wave plates for visible light, based on LCEs. These wave plates exhibit good performance over a wide range of angles between the incident linear polarization and the optical axis of the elastomer. We systematically investigate several key properties of these elastomer films, including the dependence of optical retardation on film rotation, mesogenic content, and the wavelength of the incident light.

## 1. Introduction

Controlling the polarization of light is crucial in numerous applications, including optical signal transmission, high-sensitivity measurements [1–3], fiber-optic communication, high-resolution imaging, and the detection of concealed objects [4]. Traditionally, polarized light is manipulated using birefringent crystals such as calcite, quartz, or mica, as well as mechanically stretched polymer films [5–7], which introduce the required phase difference between the fast and slow optical axes [8]. However, these approaches typically require the light to propagate through a relatively long optical path to achieve the desired phase retardation. As a result, conventional wave plates remain thick and are not well suited for the miniaturization and integration of modern optical systems [9].

The inherently high optical anisotropy of liquid crystals (LCs) makes them compelling alternatives to traditional retarders in compact photonic devices [10–12]. For example, in Ref. [13], a combination of Monte Carlo simulations and the Mueller matrix method was employed to determine the optical properties of a two-stage LC retarder system, where a lattice Hamiltonian was used to model molecular orientation distributions under various conditions.

Liquid crystal elastomers (LCEs) have recently attracted significant interest due to their potential to be used to modulate the amplitude, phase, and polarization of light. Notably, they can be synthesized as ultrathin, planar structures and they offer the advantage of a relatively simple fabrication process [14]. In addition, LCEs exhibit two well-defined responses to strain (semi-soft elasticity or a biaxial deformation) and their properties can be tuned by temperature or external fields, enabling dynamic control of light's polarization. The fabricated LCE films exhibit good elasticity, as reported in Refs. [15] and [16], with the latter providing a detailed elastic characterization of the acrylate-based LCEs investigated in this work. Furthermore, the responsiveness to external strain has been thoroughly described in Ref. [17], particularly the reduction of the effective birefringence under applied strain in these systems. This offers a unique approach for switching between a waveplate and a purely isotropic film by applying strain (this would occur at strains of ~50% in this system). Such behaviour has also been used in Ref. [18], where the strain-induced transition to the non-birefringent state is used for optical information encoding. Despite these advantages, only a limited number of studies have explored optical properties of LCEs in detail. A notable systematic investigation was reported in Ref. [19], where authors examined how the mesogenic content of acrylate-based LCEs influences the ordinary and extraordinary refractive indices, the orientational order parameter, and the phase transition temperature.

In this work, we develop and characterize acrylate-based LCE wave plates operating in the visible range in transmission mode, exploiting the optical birefringence of the elastomer. We investigate the ellipticity of output light that was initially linearly polarized and subsequently transmitted through these wave plates, as well as the azimuth of the

* Corresponding author.
*E-mail address:* g.gevorgyan@ysu.am (G. Gevorgyan).

https://doi.org/10.1016/j.optmat.2026.118241
Received 14 April 2026; Received in revised form 21 May 2026; Accepted 2 June 2026
Available online 3 June 2026

resulting polarization ellipse. Their dependence on mesogenic content, the angle between the incident polarization direction and the optical axis of the LCE, and the wavelength of the probing light are systematically analyzed. The feasibility of achieving both quarter-wave plate (QWP) and half-wave plate (HWP) functions are demonstrated.

## 2. Theoretical and numerical calculations

We investigate the polarization modulation properties of acrylate-based LCE wave plates using a rotating linear polarizer in combination with a laser power meter. This simple approach enables characterization of the output polarization state in terms of the polarization ellipse, quantified by its ellipticity and azimuth (the angle between the major axis of the ellipse and the optical axis of the elastomer). These quantities are derived from the Jones vector components of the transmitted light - specifically, the electric field amplitudes $E_x$ and $E_y$, along with the phase retardation between them [20]. Assuming fully polarized light, both the ellipticity and azimuth can be directly related to the Jones vector parameters.

It is well known that the Jones matrix of a birefringent crystal, whose optical axis is aligned with the x-axis, is given by [1].

$$M(\Delta\varphi)=\begin{bmatrix} e^{i\Delta\varphi/2} & 0 \\ 0 & e^{-i\Delta\varphi/2} \end{bmatrix} \tag{1}$$

where $\Delta\varphi = 2\pi\Delta nL/\lambda$ is the phase retardation introduced by the anisotropic medium; $\Delta n$ is the optical birefringence of the crystal (the difference between the extraordinary and ordinary refractive indices); $L$ is the thickness of the medium along the $z$-axis, which coincides with the direction of light propagation; and $\lambda$ is the wavelength of the probing light in vacuum. The Jones matrix of a HWP can be obtained from Eq. (1) by setting $\Delta\varphi = (2\,m + 1)\pi$, where $m = 0, \pm1, \pm2, \ldots$, and that of a QWP by setting $\Delta\varphi = (2\,m + 1)\pi/2$.

To determine the electric field components of light after passing through an arbitrary optical system, the Jones matrices of all intermediate optical elements must be multiplied - in the correct order - by the Jones vector representing the incident field. In particular, to analyze how the polarization state of light changes after transmission through a LCE, we multiply the Jones vector of the incident wave by the matrix in Eq. (1), assuming that the elastomer behaves as a uniaxial birefringent crystal.

It is convenient to parameterize the normalized field amplitudes as $E_x = \cos\beta$ and $E_y = \sin\beta$, where $E_x$ and $E_y$ are the x- and y-components of the transmitted electric field, and $\beta$ is the angle of LCE's optical axis with respect to the polarization direction of the incident light. Thus, the ellipticity and azimuth depend only on two variables: $\Delta\varphi$ and $\beta$. In this case, the Jones vector of linearly polarized light is given by

$$E_{in}=\begin{bmatrix} \cos\beta \\ \sin\beta \end{bmatrix} \tag{2}$$

After passing through a uniaxial anisotropic medium (Eq. (1)) - in our case, the LCE - the transmitted light acquires a Jones vector of the following form:

$$E_{out}=\begin{bmatrix} e^{i\Delta\varphi/2}\cos\beta \\ e^{-i\Delta\varphi/2}\sin\beta \end{bmatrix} \tag{3}$$

In general, the transmitted light is elliptically polarized, with its ellipticity $e$ and azimuth $\psi$ being determined using the standard formulas [1].

$$e=\tan\left(\frac{1}{2}\arcsin\left(\frac{2\mathrm{Im}\chi}{1+|\chi|^2}\right)\right),\ \psi=\frac{1}{2}\mathrm{arctg}\left(\frac{2\mathrm{Re}\chi}{1-|\chi|^2}\right) \tag{4}$$

where $\chi = E_x/E_y$, and $\psi$ is the angle between the major axis of the ellipse and the optical axis $x$. The ellipticity $e$ is defined as the ratio of the minor axis to the major axis of the polarization ellipse. For practical calculations, formulas (4) can be rewritten in a more convenient form:

$$e=-\tan\left(\frac{1}{2}\arcsin\left(\sin\Delta\varphi\,\sin 2\beta\right)\right),\ \psi=-\frac{1}{2}\mathrm{arctg}(\cos\Delta\varphi\ \mathrm{tg}2\beta) \tag{5}$$

In particular, when $\beta = 45^\circ$, we have

$$e=-\tan\left(\frac{\Delta\varphi}{2}\right),\ \psi=-45^\circ \tag{6}$$

For convenience, in our experiments we measure the quantity $f = 1/e^2$. It should be noted that when $e = \pm1$ (or equivalently, $f = 1$), the LCE functions as a QWP, whereas when $e = 0$ (or $f = \infty$) for all orientations of the incident linear polarization, the LCE behaves as an HWP. Furthermore, when a polarizer, oriented perpendicular to the initial linear polarization (Eq. (2)), and described by the Jones matrix

$$P=\begin{bmatrix} \sin^2\beta & -\sin\beta\cos\beta \\ -\sin\beta\cos\beta & \cos^2\beta \end{bmatrix} \tag{7}$$

is placed in front of the elliptically polarized light transmitted through the LCE (Eq. (3)), the resulting light becomes linearly polarized. The intensity of the transmitted light is then given by the following expression:

$$I=\sin^2(2\beta)\sin^2(\Delta\varphi/2) \tag{8}$$

In experiments, the polarization properties of acrylate-based LCE wave plates were measured at room temperature ($T = 23.5\,^\circ$C) and for light wavelengths of 532 nm and 633 nm. To interpret the results, the corresponding birefringence values $\Delta n$ for the acrylate-based LCEs are required. Recent studies [19] provide the refractive indices of the ordinary and extraordinary rays for acrylate-based LCEs at the wavelength of 589 nm, as functions of mesogenic content and temperature. From these data, the birefringence $\Delta n$ can be determined for mesogenic contents of 60%, 65%, 70%, and 75% - the compositions used in our experiments - at room temperature ($T = 23.5\,^\circ$C) and the wavelength of 589 nm. Then, the Cauchy dispersion formula [21,22] was used to obtain an analogous expression for birefringence, which is the main parameter used in the calculations:

$$\Delta n(\lambda)=A+\frac{B}{\lambda^2}+\frac{C}{\lambda^4}+\ldots \tag{9}$$

In our case, for different mesogenic contents of the LCE, the coefficients A, B, and C were determined based on the birefringence $\Delta n$ reported in Ref. [19]. We then analyzed the dependence of these coefficients on mesogenic content and extracted their values for the mesogenic contents used in this work (60%, 65%, 70%, and 75%). Using these coefficients, we calculated the corresponding birefringence $\Delta n$ for each mesogenic content at wavelengths of 532 nm and 633 nm at room temperature ($T = 23.5\,^\circ$C). The corresponding values of the coefficients A, B, and C, as well as the birefringence values, are summarized in Table 1.

It is worth noting that the birefringence in the case of 75 mol% mesogenic content is significantly higher than that observed at lower mesogenic concentrations. Our studies indicate that even a slight variation in mesogenic content can induce a transition from a nematic LCE to a frustrated smectic LCE. Specifically, LCEs with a mesogenic content above 72 mol% were found to exhibit a frustrated smectic phase.

Using parameters, presented in Table 1 and expressions (5), we can plot the dependencies of the ellipticity $f = 1/e^2$ and azimuth $\chi$ on the angle $\beta$. Recall that $f$ and $\psi$ characterize the state of polarization of linearly polarized light after transmission through the LCE. Fig. 1(a)–(d) show these dependencies for wavelengths $\lambda = 532$ nm and $\lambda = 633$ nm, and for LCEs with different mesogenic contents. Interestingly, for the LCE film thicknesses used in our experiments, it was observed that the ellipticity and azimuth vary very little from sample to sample (with different mesogenic content).

In practice, it is challenging to fabricate wave plates with perfectly

**Table 1**
Values of the coefficients A, B, and C of the Cauchy dispersion formula, together with the birefringence values of the studied LCEs for each mesogenic content at wavelengths λ = 532 nm and λ = 633 nm. The thicknesses of the corresponding samples are also indicated.

| LCE mol % | A | B (μm$^2$) | C (μm$^4$) | Δ$n$ (λ = 532 nm) | Δ$n$ (λ = 633 nm) | $L$ (μm) |
|---|---|---|---|---|---|---|
| 60 | 0.129820201 | 0.000201926 | −0.000014 | 0.13037 | 0.13024 | 140 |
| 65 | 0.135786931 | 0.000241752 | −0.000021 | 0.13638 | 0.13626 | 145 |
| 70 | 0.14788866 | 0.000281577 | −0.000028 | 0.14853 | 0.14842 | 105 |
| 75 | 0.133272956 | 0.014627565 | −0.001526 | 0.16591 | 0.16028 | 110 |

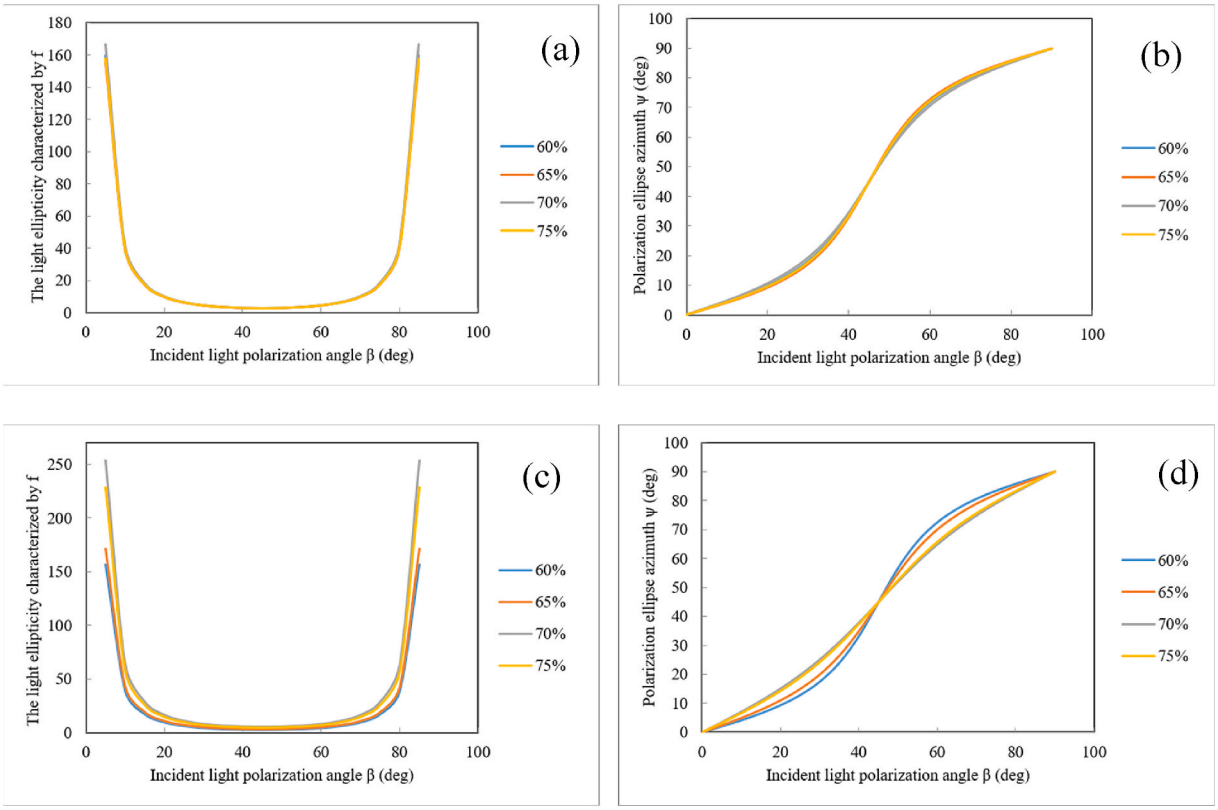


**Fig. 1.** Dependence of the calculated polarization parameters of light transmitted through LCEs on the angle between the incident linear polarization and the optical axis of the LCE for different mesogenic contents (60-75%). (a) Ellipticity of the transmitted light at λ = 532 nm, (b) Azimuth of the transmitted light at λ = 532 nm, (c) Ellipticity of the transmitted light at λ = 633 nm, (d) Azimuth of the transmitted light at λ = 633 nm.

uniform thickness across the entire surface. Nevertheless, it is straightforward to determine the thicknesses at which accurate QWP and HWP functions can be achieved for each mesogenic content, as well as for thicknesses close to those of samples used in presented experiments. Examples of such thickness values for the cases under consideration are provided in Table 2.

It should be noted that the presented thickness values correspond to the case of high-order retardation. Much thinner (some micrometers) samples would exhibit low-order retardation and better performance.

**Table 2**
Thicknesses of LCE samples that can function as quarter-wave and half-wave plates for wavelengths λ = 532 nm and λ = 633 nm, for different mesogenic contents, and corresponding retardation orders (m).

| LCE mol % | λ/4 plate for λ = 532 nm | | λ/2 plate for λ = 532 nm | | λ/4 plate for λ = 633 nm | | λ/2 plate for λ = 633 nm | |
|---|---|---|---|---|---|---|---|---|
| | $L$ (μm) | m | $L$ (μm) | m | $L$ (μm) | m | $L$ (μm) | m |
| 60 | 139.764 | 68 | 140.784 | 34 | 137.302 | 56 | 138.517 | 28 |
| 65 | 145.307 | 74 | 146.282 | 37 | 145.173 | 62 | 146.334 | 31 |
| 70 | 104.767 | 58 | 105.662 | 29 | 103.424 | 48 | 104.491 | 24 |
| 75 | 109.825 | 68 | 110.626 | 34 | 111.569 | 56 | 112.556 | 28 |

Indeed, there are studies reporting the fabrication of much thinner cholesteric liquid crystal elastomers [23,24]. However, for waveplate applications, it is essential to achieve homogeneous anisotropy and optical transparency. For the acrylate-based LCEs considered here, these conditions can be achieved for thicknesses on the order of 100 μm as shown in Ref. [19] but the fabrication methodology is not suitable for routine production of optical-quality films.

## 3. Acrylate-based LCE film preparation

The LCEs were synthesized using the following materials (see Fig. 2): 1. A6OCB (6-(4-cyanobiphenyl-4′-yloxy)hexyl acrylate), a monofunctional reactive mesogen that forms the liquid crystal polymer chain; 2. 6OCB (4-cyano-4′-hexyloxybiphenyl), a non-reactive mesogen that broadens the nematic phase range of the monomer mixture; 3. RM82 (1,4-bis-[4-(6-acryloyloxyhexyloxy)benzoyloxy]-2-methylbenzene), a bifunctional mesogenic crosslinker that contributes to the network structure; 4. EHA (2-ethylhexyl acrylate), added to increase the flexibility of the polymer backbone; 5. MBF (methyl benzoylformate), used as a UV photoinitiator.

Three powdered materials (A6OCB, RM82, and 6OCB) were weighed on an analytical balance with an accuracy of 0.1 mg and placed into a

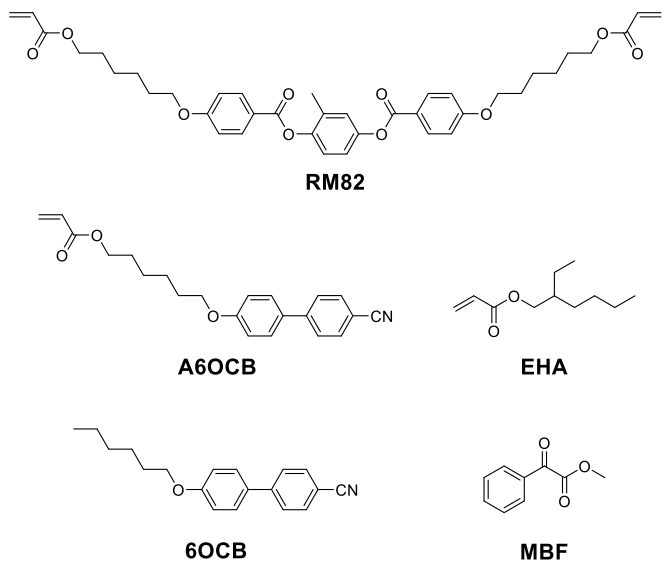


**Fig. 2.** Chemical structures of the materials used for the synthesis of acrylate-based LCEs.

2 mL glass vial. The vial was then heated to 120 °C and stirred with a magnetic stirrer at 60 rpm for 5 min to melt the powders. Subsequently, the liquid components (EHA and MBF) were added using micropipettes, and the mixture was stirred for an additional 5 min at 60 rpm and 50 °C. The resulting mixture was poured into a pre-fabricated cell [14] with a thickness of 100 μm, maintained at 50 °C (in the isotropic phase), and slowly cooled to room temperature. This cooling induced the transition of the LC to the nematic phase, with molecules aligning along a pre-treated planar direction. The cell thickness was chosen as a compromise between achieving reasonable alignment of the LC precursor mixture and the ease of handling of the final LCE film; films with smaller thickness can be fabricated by using thinner cells. To cure the precursor mixture, the cell was then exposed to low-intensity UV radiation (2.5 mW/cm$^2$) for 2 h to achieve polymerization. After polymerization, the cell was immersed in 2-propanol to swell the elastomer and separate it from substrates. Prior to experiments, the separated LCE samples were dried overnight. The compositions of LCE components are listed in Table 3.

**Table 3**
Chemical composition of the LCEs used in the experiments. Both the initial monomer mixture and the final LCE compositions are shown.

| Mesogenic Content (mol. %) | Component | Quantity (mol. %) | |
|---|---|---|---|
| | | Monomer Mixture | Final LCE |
| 60 | RM82 | 3.5 | 7.7 |
| | A6OCB | 23.7 | 52.3 |
| | 6OCB | 54.6 | - |
| | EHA | 16.7 | 36.7 |
| | MBF | 1.5 | 3.3 |
| 65 | RM82 | 3.5 | 7.7 |
| | A6OCB | 26.0 | 57.3 |
| | 6OCB | 54.6 | - |
| | EHA | 14.4 | 31.7 |
| | MBF | 1.5 | 3.3 |
| 70 | RM82 | 3.5 | 7.7 |
| | A6OCB | 28.3 | 62.3 |
| | 6OCB | 54.6 | - |
| | EHA | 12.1 | 26.7 |
| | MBF | 1.5 | 3.3 |
| 75 | RM82 | 3.5 | 7.7 |
| | A6OCB | 30.6 | 67.3 |
| | 6OCB | 54.6 | - |
| | EHA | 9.9 | 21.7 |
| | MBF | 1.5 | 3.3 |

The polarizing optical microscopy (POM) images of one of the fabricated LCEs is shown in Fig. 3.

## 4. Description of the experimental setup

The experiments were conducted using acrylate-based LCEs with varying mesogenic contents, employing a measurement system consisting of a polarizer and a laser power meter (S120VC, Thorlabs). The experimental setup is illustrated in Fig. 4. This setup allows determination of the polarization state of light in the form of a polarization ellipse, providing numerical values for the ellipticity and azimuth. Elastomers with mesogenic contents of 60%, 65%, 70%, and 75% were used in the study, all exhibiting uniform planar molecular alignment along the *x*-axis (see Fig. 4).

A linearly polarized laser beam first passes through a commercial rotating HWP, positioned perpendicular to the beam propagation, allowing controlled rotation of the polarization direction while maintaining linearity. The beam then traverses the LCE sample, also oriented perpendicular to the beam, where it experiences phase retardation. To evaluate this retardation, a rotating linear polarizer and laser power meter are placed after the sample, enabling measurement of the polarization ellipticity of the transmitted beam. If the output remains linearly polarized for all incident polarization directions, the sample behaves as an HWP; if the output is circularly polarized, the sample functions as a QWP. Intermediate cases result in elliptical polarization. All experiments were performed at room temperature (23.5 °C).

## 5. Polarization properties of LCE films

To verify that the LCE films function as wave plates, we first studied the dependence of the output light ellipticity on the angle β between the polarization of the incident light and the optical axis of the LCE film. During the experiments, β was varied by rotating the commercial HWP. For each angle, the ellipticity *f*, defined as the ratio of the power along the major and minor axes of the output polarization ellipse, as well as the azimuth, were measured. These measurements allowed us to plot the dependence of the output ellipticity and azimuth on the angle β.

Experiments were performed for LCE samples with mesogenic contents of 60%, 65%, 70%, and 75%, and for light wavelengths of 532 nm (DPSS laser) and 633 nm (He–Ne gas laser). The results are shown in Fig. 5(a) and Fig. 5(b) for 532 nm, and Fig. 5(c) and Fig. 5(d) for 633 nm. The graphs indicate that linearly polarized light remains linear at $\beta = 0^\circ$ and $\beta = 90^\circ$, as expected (see Fig. 1). The minimum ellipticity occurs at $\beta = 45^\circ$, where the LCE behaves most closely to a QWP. This behavior is consistent across all mesogenic contents.

Since the measured values can vary depending on the point of the sample through which the laser passes, multiple measurements were performed at different positions, and the results were averaged. The graphs present these averaged values.

By superimposing the experimental curves from Fig. 5(a–d) onto the corresponding theoretical predictions, a good agreement is observed. The results indicate that, for a wavelength of 532 nm, the ellipticity minima are 2.47, 2.30, 2.73, and 2.40 for LCE samples with mesogenic contents of 60%, 65%, 70%, and 75%, respectively. For a wavelength of 633 nm, the corresponding minima are 2.33, 2.83, 5.54, and 4.73 for the same series of mesogenic contents.

## 6. Results of the experiment to evaluate LCE's transmittance

To evaluate the optical transparency of the studied LCE wave plates, transmittance measurements were performed using the experimental setup shown in Fig. 4, but without a polarizer. A linearly polarized laser beam first passed through a commercial rotating HWP, positioned perpendicular to the beam propagation, allowing rotation of the polarization direction while maintaining linearity. The beam then traversed the LCE sample, oriented perpendicular to the propagation direction.

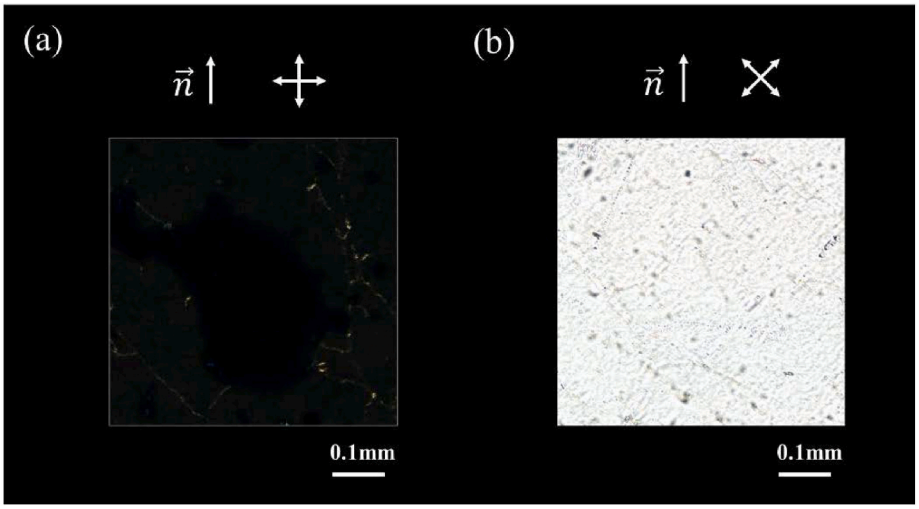


**Fig. 3.** POM images of the fabricated LCE (70 mol%) obtained using a Leica Microsystems DMi8 microscope between crossed polarizers. The images demonstrate the planar alignment of the sample, with the director oriented at (a) 0° relative to one of the polarizers and (b) 45° relative to the polarizers.

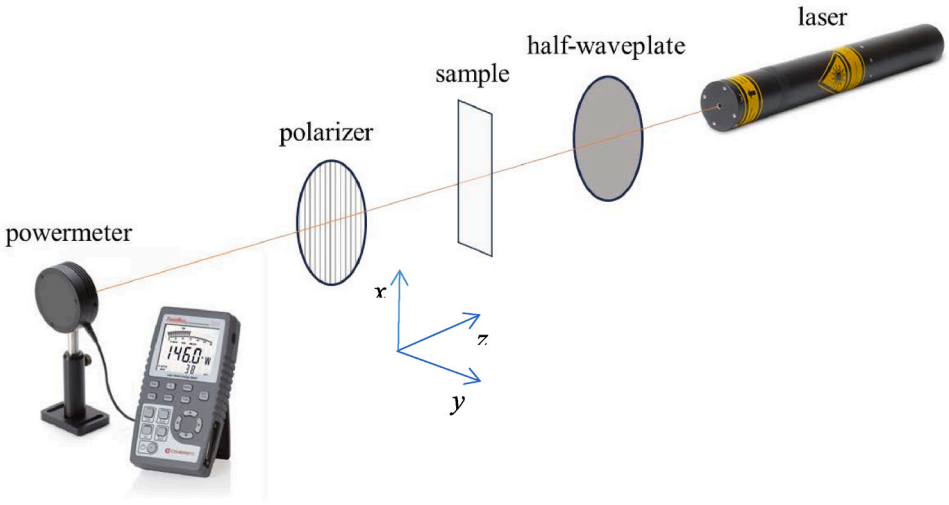


**Fig. 4.** Schematic diagram of the experimental setup used to measure the polarization properties of acrylate-based LCE wave plates.

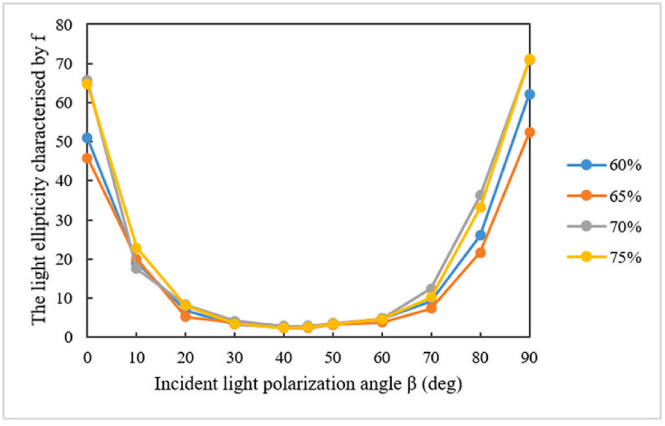


**Fig. 5(a).** Dependence of the transmitted light ellipticity on the angle between the incident laser polarization and the optical axis of the LCE sample, for four mesogenic contents (60%, 65%, 70%, 75%) at a wavelength of 532 nm.

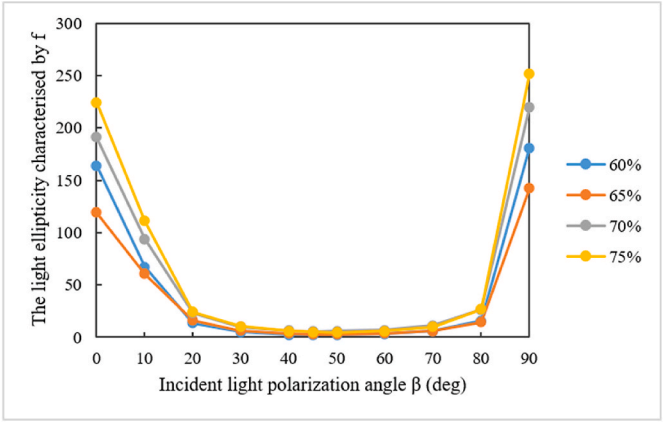


**Fig. 5(b).** Dependence of the transmitted light ellipticity on the angle between the incident laser polarization and the optical axis of the LCE sample, for four mesogenic contents (60%, 65%, 70%, 75%) at a wavelength of 633 nm.

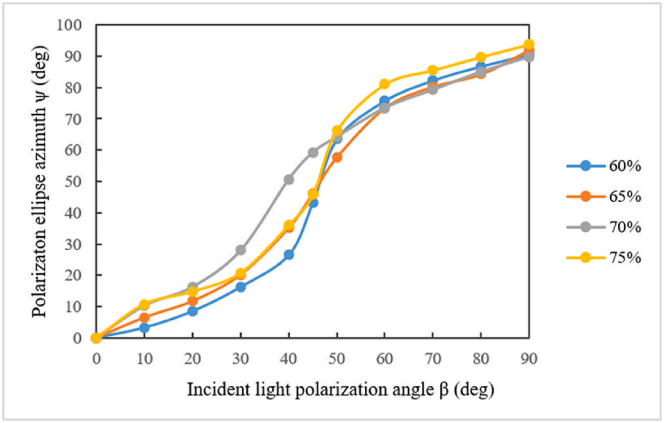


**Fig. 5(c).** Dependence of the azimuth of the transmitted light on the angle between the incident laser polarization and the optical axis of the LCE sample, for four mesogenic contents (60%, 65%, 70%, 75%) at a wavelength of 532 nm.

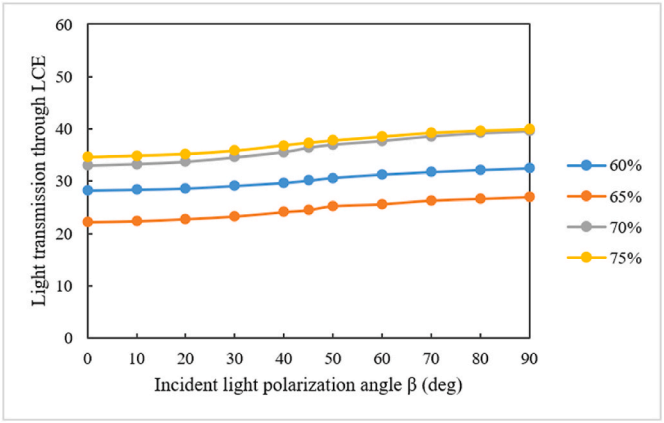


**Fig. 6(a).** Dependence of the transmittance coefficient (%) on the angle between the incident light polarization and the optical axis of the LCE sample, for four mesogenic contents (60%, 65%, 70%, 75%) at a wavelength of 532 nm.

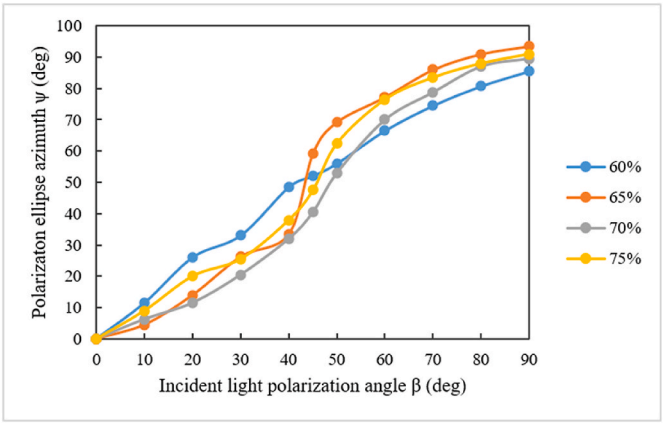


**Fig. 5(d).** Dependence of the azimuth of the transmitted light on the angle between the incident laser polarization and the optical axis of the LCE sample, for four mesogenic contents (60%, 65%, 70%, 75%) at a wavelength of 633 nm.

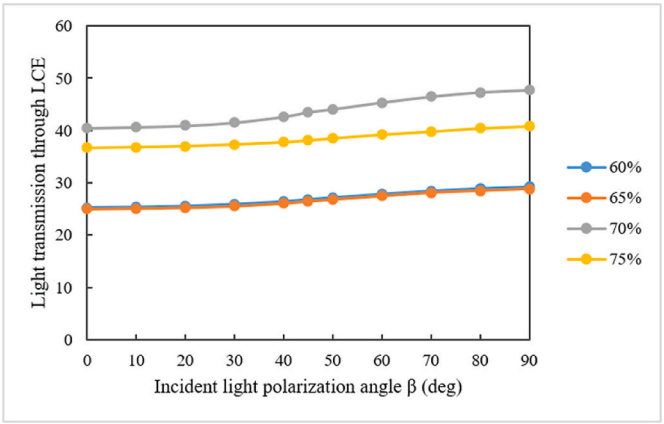


**Fig. 6(b).** Dependence of the transmittance coefficient (%) on the angle between the incident light polarization and the optical axis of the LCE sample, for four mesogenic contents (60%, 65%, 70%, 75%) at a wavelength of 633 nm.

The transmitted laser power was measured using a laser power meter placed after the sample. However, in this case, a diaphragm was placed in front of the power meter so that the scattered part is blocked and only the central part of the beam (approximately 2 mm in diameter) is detected. This results in a reduction of the absolute transmittance value but provides more detailed information about the central region of the beam, which is more relevant for studying LCEs as waveplates. Without the diaphragm, and with a well-aligned film, the transmittance of this kind of LCE exceeds 90% [19] and can be even higher for thinner samples. The successful fabrication of such films could make them suitable for use as waveplates. For each measurement, the initial laser power was recorded before installing the LCE, and then the transmitted power was measured at different orientations of the HWP. The transmittance coefficient of the sample was calculated as the ratio of the transmitted power to the initial power. All experiments were conducted at room temperature ($T = 23.5\,^{\circ}C$).

Using the measurement data, graphs were plotted to show the dependence of the transmittance coefficient on the angle between the incident light polarization and the optical axis of the LCE. Experiments were performed for samples with four different mesogenic contents (60%, 65%, 70%, and 75%) and for light wavelengths of 532 nm and 633 nm. The resulting data are presented in Fig. 6(a) and Fig. 6(b) for 532 nm and 633 nm, respectively. Here again, the graphs represent the spatially averaged values.

The results indicate that samples with mesogenic contents of 70% and 75% exhibit higher transmittance. This observation is consistent with the fact that higher mesogenic content corresponds to a higher orientational order parameter [19], which enhances optical transparency. In general, as mentioned earlier, the reduced transmittance arises from scattering caused by imperfect molecular ordering; this effect is exaggerated in the films with lower mesogenic content as they were considerably thicker (~140 μm rather than ~100 μm) and so the alignment is less good. In theoretical calculations, transmittance is assumed for ideal samples, where 100% transmission is expected.

## 7. Transmission of LCE between HWP and polarizer

Next, the transmittance of LCE samples placed between HWP and a polarizer was measured using the experimental setup shown in Fig. 4. A linearly polarized laser beam first passed through a rotatable commercial HWP, positioned perpendicular to the beam propagation. The beam then traversed the LCE sample, also oriented perpendicular to the propagation direction, and subsequently passed through a polarizer crossed relative to the initial polarization of the incident light. The transmitted light power was recorded using a laser power meter.

For each measurement, the initial laser power was first recorded with the polarizer parallel to the incident light's polarization. Then, the polarizer was crossed (rotated at 90°), the LCE sample was introduced, and the transmitted power was measured for different angles between the incident polarization and the optical axis of the LCE. To ensure that

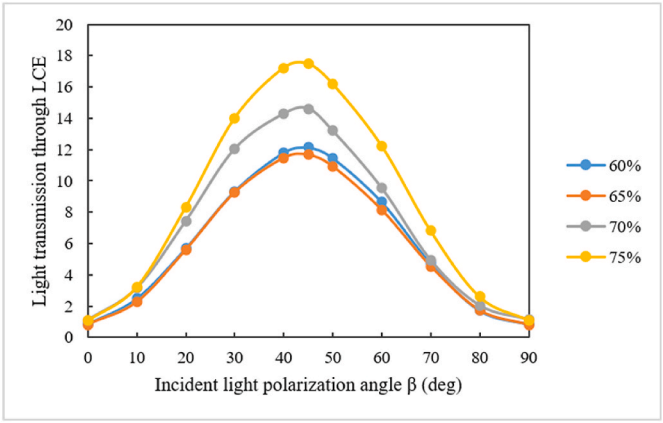


**Fig. 7(a).** Dependence of the transmittance (%) of LCE + polarizer system on the angle between the incident polarization and the optical axis of the LCE, measured with the polarizer crossed relative to the HWP (incident polarization), for four mesogenic contents (60%, 65%, 70%, 75%) at a wavelength of 532 nm.

the laser beam passed through the same point on the sample in all measurements, the HWP and the polarizer were rotated while keeping them crossed, rather than rotating the sample. The transmittance coefficient of the sample between crossed polarizers was calculated as the ratio of transmitted power to initial power. All experiments were conducted at room temperature ($T = 23.5\,^{\circ}C$).

Graphs were plotted to show the dependence of the transmittance coefficient on the angle between the incident laser polarization and the optical axis of the LCE. Experiments were performed for samples with four mesogenic contents (60%, 65%, 70%, 75%) and for light wavelengths of 532 nm and 633 nm. The results are presented in Fig. 7(a) and Fig. 7(b), corresponding to 532 nm and 633 nm, respectively. Here again, multiple measurements were taken at different positions of the LCE, and the results were averaged. The graphs represent these averaged values.

Here, the transmittance is again higher for samples with mesogenic contents of 70% and 75%, indicating a higher orientational order parameter of the LC molecules in these samples, which leads to improved optical transmission. Notably, the results shown in Fig. 7(a) and (b) are in excellent agreement with the theoretical dependence described by Eq. (8).

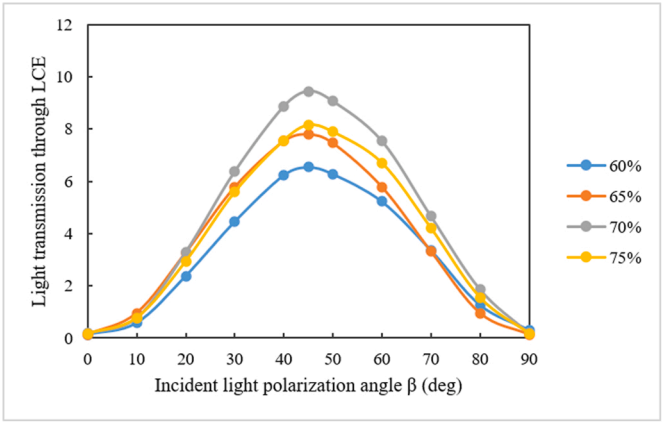


**Fig. 7(b).** Dependence of the transmittance (%) of LCE + polarizer system on the angle between the incident polarization and the optical axis of the LCE, measured with the polarizer crossed relative to the HWP (incident polarization), for four mesogenic contents (60%, 65%, 70%, 75%) at a wavelength of 633 nm.

## 8. Conclusion

This paper proposes the use of acrylate-based LCEs for the fabrication of thin-film, soft-elastic wave plates. By selecting the appropriate thickness and mesogenic content of the LCE, the desired phase retardation can be achieved for a given wavelength. In particular, QWPs can be designed to convert circularly polarized light into linearly polarized light and vice versa, while HWPs can invert the polarization direction of linearly polarized light or convert right-circularly polarized light into left-circularly polarized light. These wave plates operate effectively over a wide range of angles between the initial linear polarization and the optical axis of the elastomer. The developed wave plates are thin and operate in transmission mode.

In this study, we investigated elastomeric films which were fabricated without special attention being paid to ensure a uniform thickness or optimum LC alignment. Even in these films, the optical performance is of interest in terms of enabling inexpensive optical components with facile fabrication methodology. Films with much higher transparency and better performance can be obtained if the thickness is decreased to several micrometers and this will be the focus of our future research. Achieving very thin, uniform films would reduce sensitivity of the wave plates to variations in thickness, wavelength, and mesogenic content, further enhancing their performance and reliability.

Given their thin-film nature, mechanical flexibility, and tunable optical anisotropy, such LCE-based wave plates present a promising alternative for controlling the polarization state of electromagnetic waves, offering advantages for the integration and miniaturization of optical systems. Thus, they hold strong potential for applications in AR/VR headsets, biomedical imaging, fiber-optic communication systems, astronomical instrumentation, semiconductor processing, aerospace sensing, and other technologies requiring precise polarization control.

## Funding

The research by K.M., G.G., M.H., T.G. and R.H. was supported by the Higher Education and Science Committee of RA, in the frames of the research project No. 21AG–1C088.

S.B. and H.G. acknowledge funding from the Engineering and Physical Sciences Research Council, grant number EP/V054724/1.

## CRediT authorship contribution statement

**Karine Margaryan:** Data curation, Investigation. **Gevorg Gevorgyan:** Data curation, Investigation, Supervision, Validation, Visualization, Writing – original draft. **Mariam Hakobyan:** Data curation, Visualization. **Tigran Galstian:** Data curation, Validation. **Stuart Berrow:** Data curation, Writing – original draft. **Helen Gleeson:** Conceptualization, Supervision, Writing – original draft. **Rafik Hakobyan:** Conceptualization, Supervision, Validation, Writing – original draft.

## Declaration of competing interest

The authors declare that they have no known competing financial interests or personal relationships that could have appeared to influence the work reported in this paper.

## Data availability

Data will be made available on request.

## References

[1] Pochi Yeh, Claire Gu, Optics of Liquid Crystal Displays, second ed., Wiley, 2010. ISBN: 9780470181768.
[2] B.Q. Lin, J. Wu, X. Da, W. Li, J. Ma, Appl. Phys. A 123 (43) (2017) 1, https://doi.org/10.1007/s00339-016-0673-8.

[3] D. Chen, H. Zeng, Y. Qi, H. Liu, Q. Xue, X. Sun, Opt. Eng. 61 (2) (2022), https://doi.org/10.1117/1.OE.61.2.025104, 025104-1.
[4] J.Q. Yang, T. Lan, Appl. Opt. 58 (4) (2019) 782, https://doi.org/10.1364/AO.58.000782.
[5] Y. Li, J. Luo, X. Li, M. Pu, X. Ma, X. Xie, J. Shi, X. Luo, IEEE Photon. J. 12 (2) (2020) 4600410, https://doi.org/10.1109/JPHOT.2020.2971592.
[6] E. Hecht, A. Zajac, Optics, fourth ed., Addison–Wesley, 1979. ISBN: 0321188780.
[7] G.D. Walter, V. William, Handbook of Optics Sponsored by OSA, McGraw-Hill, 1978. ISBN: 0070477108.
[8] F. Ding, Z. Wang, S. He, V.M. Shalaev, A.V. Kildishev, ACS Nano 9 (4) (2015) 4111, https://doi.org/10.1021/acsnano.5b00218.
[9] Y.M. Yang, W. Wang, P. Moitra, I.I. Kravchenko, D.P. Briggs, J. Valentine, Nano Lett. 14 (3) (2014) 1394, https://doi.org/10.1021/nl4044482.
[10] G. Yang, Z. Zheng, H. Li, et al., Method to reduce side lobes of multistage lyot filters, Appl. Opt. 49 (8) (2010) 1280–1287, https://doi.org/10.1364/AO.49.001280.
[11] O. Aharon, I. Abdulhalim, Liquid crystal lyot tunable filter with extended free spectral range, Opt. Express 17 (14) (2009) 11426–11433, https://doi.org/10.1364/OE.17.011426.
[12] G. Kopp, M.J. Derks, D.F. Elmore, et al., Tunable liquid-crystal filter for solar imaging at the He i 1083-nm line, Appl. Opt. 36 (1) (1997) 291–296, https://doi.org/10.1364/AO.36.000291.
[13] Y. Emül, Monte carlo simulations for tuning optical properties in a two-stage liquid crystal retarder system via mueller matrix method, Liq. Cryst. 52 (3–4) (2025) 212–219, https://doi.org/10.1080/02678292.2024.2423375.
[14] S.R. Berrow, T. Raistrick, R.J. Mandle, H.F. Gleeson, Polymers 16 (2024) 1957, https://doi.org/10.3390/polym16141957.
[15] Lu, L., Chen, X., Liu, W., Li, H., Li, Y., & Yang, Y., Liq. Cryst., 50(6), 1025–1034. https://doi.org/10.1080/02678292.2023.2200266.
[16] G.S. Gevorgyan, M.L. Sargsyan, M.R. Hakobyan, M. Reynolds, H.F. Gleeson, R. S. Hakobyan, Polymers 17 (5) (2025) 614, https://doi.org/10.3390/polym17050614.
[17] Z. Wang, T. Raistrick, A. Street, M. Reynolds, Y. Liu, H.F. Gleeson, Materials 16 (1) (2023) 393, https://doi.org/10.3390/ma16010393.
[18] Z. Wang, T. Raistrick, et al., Mater. Horiz. 13 (2026) 2568–2582, https://doi.org/10.1039/D5MH01817J.
[19] E.J. Cooper, M. Reynolds, T. Raistrick, S.R. Berrow, E.I.L. Jull, V. Reshetnyak, D. Mistry, H.F. Gleeson, Macromolecules 57 (2024) 2030, https://doi.org/10.1021/acs.macromol.3c02226.
[20] M. Born, E. Wolf, Principles of Optics, Pergamon, 2019, https://doi.org/10.1017/9781108769914.
[21] A.L. Cauchy, MEmoire Sur La Dispersion De La Lumi'Ere (Prague: Calve), 1836.
[22] J. Weirich, J. Lægsgaard, L. Wei, T.T. Alkeskjold, T.X. Wu, S.-T. Wu, A. Bjarklev, Opt. Express 18 (5) (2010) 4074–4087, https://doi.org/10.1364/OE.18.004074.
[23] M. Zhang, B. Li, W. Liu, Y. Li, Y. Yang, New J. Chem. 48 (2024) 17287–17293, https://doi.org/10.1039/D4NJ02983F.
[24] R. Li, J. Yan, W. Liu, Y. Li, Y. Yang, J. Mater. Chem. C (2026), https://doi.org/10.1039/D6TC00115G.